A Compact Ultra-High Brightness Cryogenic C-Band RF Gun for Ultra-Fast Electron Diffraction Applications

C. Pennington[1], G. Lawler[1], F. Bosco[1], A. Bartnik[2], J. Jimenez-Zepeda[1], S. Tantawi [3], J. Maxson[2], J. Rosenzweig[1]
[1]University of California, Los Angeles, Los Angeles, CA 90095, USA
[2]Cornell University, Ithaca, NY 14853, USA
[3]Arizona State University, Tempe, AZ 85281, USA

Abstract

We present the current status of the Cryogenic Brightness-Optimized Radiofrequency Gun (CYBORG), a compact high-field cryogenic C-band photoinjector beamline for ultrafast electron diffraction applications. Using General Particle Tracer (GPT) simulations together with multi-objective optimizations, we investigate the performance of the beamline as a high brightness source for MeV ultrafast electron diffraction (UED). The optimization targets were minimization of the electron bunch length and normalized 4D transverse emittance at the sample plane, with emphasis on high-brightness single-shot UED operation. For practical cathode source sizes of 40 µm, optimized solutions achieved brightness values approaching 10^{14} A/m^2 with bunch durations near 50 fs. Simulations using micron-scale source sizes demonstrated brightness exceeding 10^{16} A/m^2 with a bunch length of less than 20 fs at the sample, illustrating the performance potential of high-field cryogenic photoinjectors combined with low mean transverse energy photocathodes. Diffraction simulations further indicate that, despite post-sample space-charge broadening, the essential diffraction features remain intact in the low-charge operating regime considered here. These results demonstrate the potential of normal-conducting cryogenic photoinjectors for compact high-brightness MeV UED operation.

INTRODUCTION

Photocathode-based ultrafast electron diffraction (UED) systems require electron beams with high brightness, femtosecond-scale duration, and sufficient charge for single-shot or high signal-to-noise measurements. Existing UED beamlines are primarily based on DC and room-temperature normal-conducting RF (NCRF) photoinjectors, each offering distinct advantages in beam quality, coherence, and achievable energy [1, 2]. Recent advances in cryogenic NCRF photoinjectors have opened a promising path toward significantly enhanced beam brightness through operation at substantially higher accelerating fields and reduced intrinsic emittance [3–5].

Cryogenic copper RF cavities operated at temperatures of ~27–77 K exhibit reduced RF losses, increased conductivity, and improved mechanical hardness, enabling operation at electric fields substantially exceeding those achievable in room-temperature copper structures [6, 7]. In parallel, low-temperature photocathode operation can suppress excess momentum during photoemission, reducing intrinsic emittance and improving beam quality. Together, these effects make cryogenic RF photoinjectors attractive candidates for next-generation high-brightness UED sources.

The CrYogenic Brightness Optimized Radio-frequency Gun (CYBORG) beamline at UCLA was recently commissioned as a high-field cryogenic RF photoinjector platform compatible with insertable cathode plugs [8]. In this work, we investigate the expected UED performance of the CYBORG beamline using beam dynamics simulations based on the present and near-term machine configuration. The study focuses on optimization of ultrafast, high-brightness operating points relevant to MeV-UED applications.

To quantify beamline performance, we employ the five-dimensional brightness

$$B_{5D} = \frac{Q}{\epsilon_{nx}\epsilon_{ny}\sigma_t}, \tag{1}$$

where Q is the bunch charge, ϵ_{nx} and ϵ_{ny} are the normalized transverse emittances, and σ_t is the rms bunch duration. Assuming radial symmetry, we define the normalized four-dimensional transverse emittance as

$$\epsilon_{4D} = \sqrt{\epsilon_{nx}\epsilon_{ny}}, \tag{2}$$

allowing the brightness expression to be recast as

$$B = \frac{Q}{(\epsilon_{4D})^2\sigma_t}. \tag{3}$$

THE CYBORG BEAMLINE

The CYBORG beamline at UCLA is a compact cryogenic C-band photoinjector platform designed for high-brightness beam studies and ultrafast electron diffraction applications. The present beamline configuration is shown in Fig. 2. The injector consists of a 5712 MHz half-cell cryogenic copper cavity with re-entrant nose cones designed to enhance the on-axis accelerating field and maximize shunt impedance [8, 9]. The high shunt impedance achievable in cryogenic copper cavities is particularly advantageous for compact accelerator systems, as large accelerating fields can be obtained with comparatively modest RF power. This operating regime enables relativistic beam generation in a substantially reduced footprint relative to conventional MeV-UED facilities while maintaining the high brightness required for ultrafast diffraction applications. Electromagnetic field maps used in the beam dynamics simulations were obtained from COMSOL calculations.

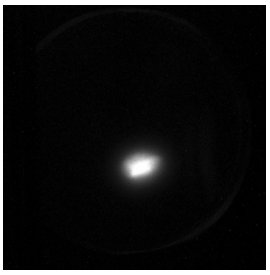

(a)

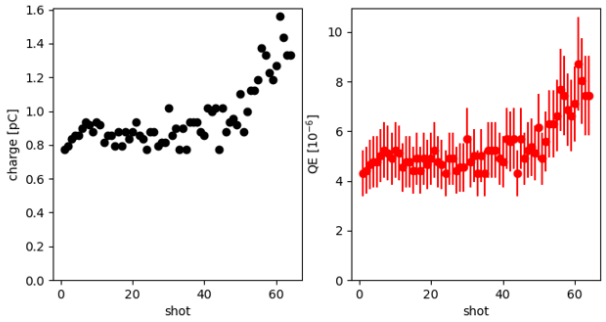

(b) (c)

Figure 1: (a) First observed photoelectron beam image from the cryogenic RF photoinjector. (b) Measured bunch charge during the first sequence of shots. (c) Quantum efficiency evolution during the same measurement.

The gun is operated inside a cryostat and cooled using closed-cycle cryocoolers. A downstream solenoid provides transverse focusing, with beam diagnostics positioned downstream of the interaction region. The beam dynamics studies presented here assume a peak launch field of 180 MV/m, corresponding to the anticipated operating point following implementation of a pulse-compression system currently under development.

A load-lock compatible cathode geometry is incorporated into the gun design to support future operation with low mean transverse energy photocathodes relevant to high-brightness UED applications.

Initial dark current studies of the machine were previously reported in [9, 10]. More recently, we demonstrated the first photoelectron beam from the cryogenic normal-conducting RF gun shown in Fig. 1(a). Operating with a copper photocathode, we measured a bunch charge of approximately 1 pC and a quantum efficiency on the order of 5×10^{-6}. While this quantum efficiency is modest, it is within the range commonly reported for copper photocathodes operated near threshold and under non-optimized surface conditions [11]. Cryogenic operation can further modify the photoemission response through changes in the electron distribution and effective emission threshold [12].

LOAD-LOCK CATHODE INTEGRATION

A central feature of the CYBORG beamline is the integration of a load-lock compatible cathode geometry designed to support advanced low mean transverse energy (MTE) photocathodes. The system enables insertion of removable cathode plugs while maintaining ultra-high vacuum conditions, allowing operation with air-sensitive semiconductor photocathodes and future nanostructured emitters relevant to high-brightness UED applications.

The optimization studies presented here indicate that the attainable beam brightness is strongly enhanced by reductions in both MTE and effective emission area. In particular, the micron-scale source size regime explored in the simulations approaches normalized 4D emittances near the nanometer scale and brightness values exceeding 10^{16} A/m^2. Although such operating conditions remain experimentally challenging, they motivate development of advanced localized emission cathodes compatible with the CYBORG demountable back-plane.

The combination of high extraction fields and low-MTE photocathodes provides a path toward experimentally accessing ultrafast electron beam regimes that remain relatively unexplored in compact NCRF photoinjectors.

SIMULATION STUDIES OF UED BEAMLINE OPTIMIZATIONS

Multi-objective optimizations coupled to General Particle Tracer (GPT) simulations were performed to identify operating points of the CYBORG beamline optimized for ultrafast electron diffraction. The optimization objectives were minimization of the bunch length and normalized 4D transverse emittance at the sample plane. Beamline parameters varied during the optimization are listed in Table 1. Each optimization used a population size of 1000 and evolved until the Pareto front converged over successive generations.

Three representative mean transverse energy (MTE) values were considered: 150 meV for metallic copper cathodes under above-threshold UV illumination [13], 70 meV for near-threshold semiconductor emission [14], and 35 meV for cryogenic semiconductor cathodes [15, 16]. A delivered bunch charge of 10^5 electrons ($\approx$ 16 fC) was imposed at the sample plane for all optimizations. The transverse beam size

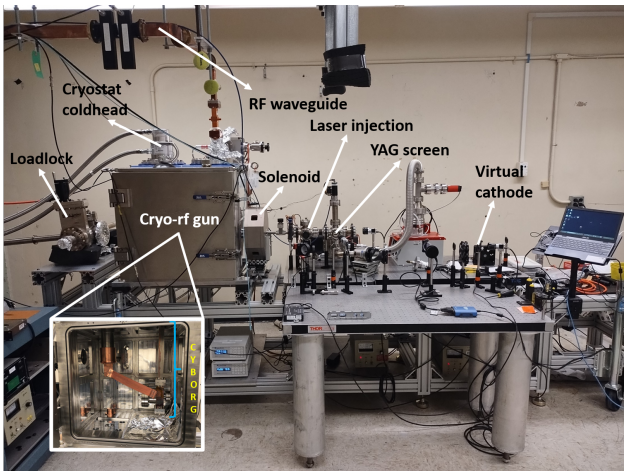

Figure 2: Current configuration of the CYBORG beamline. The RF gun within the cryostat and the connection with the cold head are shown.

at the sample, located 1.5 m downstream of the injector, was constrained to remain below 100 µm.

Figure 3 shows the resulting Pareto fronts of normalized 4D emittance as a function of bunch length for cathode source sizes of 40 and 1 µm. Lower MTE systematically improves the attainable emittance in both operating regimes. For the practical source size of $\sigma_{x,i} = 40\,\mu\text{m}$, representative optimized solutions with bunch lengths near 50 fs achieve normalized 4D emittances of approximately 15 nm at the sample plane, corresponding to a 5D brightness of $B_{5D} \approx 1.0 \times 10^{14}$ A/m^2. Solutions with bunch lengths approaching 20 fs were also identified without use of a dedicated bunching cavity, with compression arising from injector fields and collective effects alone.

Reducing the source size to $\sigma_{x,i} = 1\,\mu\text{m}$ significantly extends the attainable brightness frontier. In this regime, the normalized 4D emittance approaches 1 nm for longer bunch lengths, while representative compressed solutions with bunch lengths below 30 fs reach brightness values exceeding 10^{16} A/m^2. The relative benefit of reducing MTE becomes less pronounced at the micron scale, indicating that geometric source size rather than intrinsic thermal spread becomes the primary limitation.

This behavior suggests a transition from a thermally dominated emittance regime toward one increasingly governed by source geometry and collective effects. In the extreme focusing regime, reductions in intrinsic thermal spread alone become insufficient to fully determine the achievable beam brightness. Further performance improvements may therefore require advances in localized emission control, cathode fabrication, and mitigation of nonlinear space-charge dynamics.

An important feature of the optimized solutions is that bunch lengths below 20 fs were achieved without use of a dedicated bunching cavity. In these operating points, longitudinal compression arises directly from the injector fields and collective beam dynamics, indicating that compact cryogenic photoinjectors may access ultrafast operating regimes with substantially simplified beamline layouts compared with conventional MeV-UED facilities.

Compared with conventional DC-UED systems, the high extraction fields achievable in cryogenic NCRF photoinjectors provide stronger mitigation of space-charge induced emittance growth in the early stages, while simultaneously enabling MeV beam energies favorable for increased sample penetration depth and reduced temporal broadening during propagation. The optimization results presented here therefore suggest that compact cryogenic RF injectors may provide an attractive intermediate regime combining the high coherence traditionally associated with DC-based systems with the relativistic operating advantages of MeV-UED beamlines.

Table 1: Beamline simulation parameters

Beamline Parameter	Range
Spot size on cathode	[0.9, 80] µm
Gun phase offset ($\Delta\phi$)	[-15,15] °
Initial bunch length	[50, 300] fs
Solenoid position	[0.24, 1.0] m
Solenoid strength	[0.0, 3.0] T

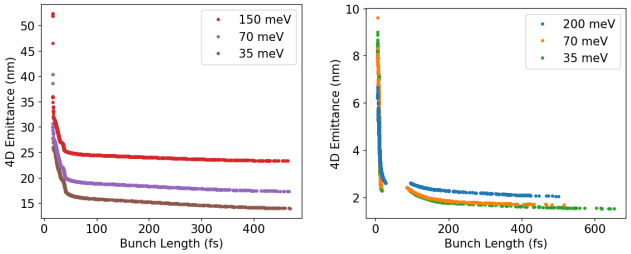

(a) $\sigma_{x,i} = 40\,\mu\text{m}$ (b) $\sigma_{x,i} = 1\,\mu\text{m}$

Figure 3: Pareto front optimizations of normalized 4D emittance versus bunch length for electron beam source sizes of 40 and 1 µm using representative photocathode MTE values.

DISCUSSION

Although the beam parameters are optimized at the sample plane, collective Coulomb forces remain important during downstream propagation of the diffracted beamlets. Diffracted electrons continue to interact with the intense unscattered core during the drift after the sample, which can broaden and distort Bragg features relative to the ballistic case. These post-sample collective effects are particularly relevant in single-shot high-brightness UED, where the large charge density can degrade resolution [2, 17].

To assess these effects, analytic diffraction simulations were performed using GPT particle distributions extracted at the sample plane for the optimized 1 µm, 35 meV operating point. Diffraction was modeled by applying momentum kicks corresponding to a graphene lattice, followed by GPT propagation with and without space charge. The downstream evolution was simulated using a Barnes–Hut tree algorithm with 5×10^4 macroparticles and opening angle parameter $\theta = 0.3$.

Figure 4 compares the diffraction evolution with and without space charge after the sample. Immediately downstream of the sample, the diffracted beamlets strongly overlap with the dense unscattered core, leading to broadening and distortion of the Bragg features in the space-charge-on case. However, for the low bunch charges considered here ($Q \approx 15$ fC), the essential diffraction structure remains preserved despite the presence of collective effects. As the beam propagates downstream, geometric separation of the diffracted beamlets from the central beam reduces the interaction strength, allowing the Bragg peak centroids to remain distinguishable despite residual broadening.

An important feature of the optimized solutions is the formation of a micron-scale waist at the sample plane, producing locally high charge densities and enhanced post-sample space-charge forces immediately downstream of the interaction region. These results suggest that, although the ultrahigh-brightness operation increases sensitivity to post-sample collective effects, the low-charge regime considered

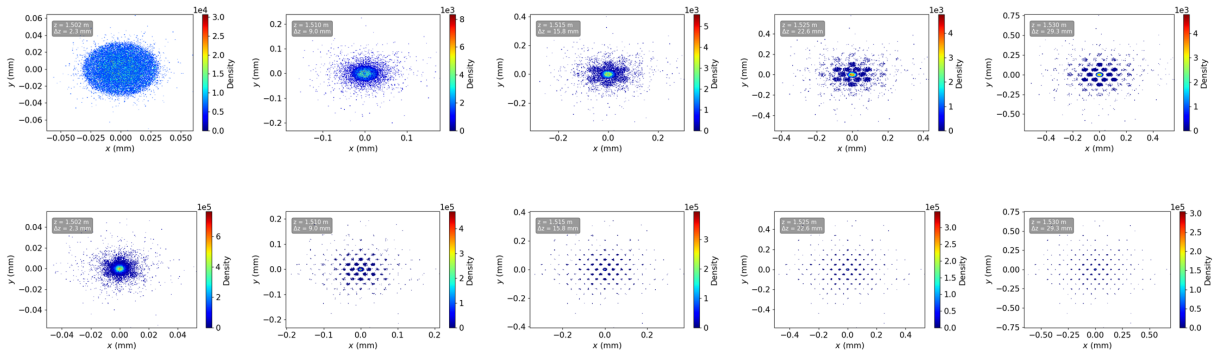

Figure 4: Evolution of diffraction beamlets downstream of the sample with and without post-sample space charge forces. Space charge broadens and distorts the Bragg features immediately after the sample, while the low bunch charge and geometric separation during propagation limit degradation of the essential diffraction structure downstream.

here remains compatible with preservation of the essential diffraction information, including Bragg peak position and width. Detector placement and drift length optimization may therefore play an important role in mitigating the impact of post-sample collective effects in ultrahigh-brightness UED experiments.

SUMMARY AND CONCLUSION

We presented the current status of the Cryogenic Brightness-Optimized Radiofrequency Gun (CYBORG), a compact cryogenic C-band photoinjector beamline, together with simulation studies of its application to ultrafast electron diffraction. For practical source sizes of 40 µm, optimized solutions achieved normalized 4D emittances near 15 nm with ~50 fs bunch durations, corresponding to brightness values approaching 10^{14} A/m^2. Simulations using micron-scale source sizes demonstrated brightness exceeding 10^{16} A/m^2, illustrating the performance potential of high-field cryogenic photoinjectors combined with low-MTE photocathodes.

The optimized solutions further indicate that sub-20 fs bunches can be achieved without a dedicated bunching cavity, with compression arising directly from injector fields and collective beam dynamics. Diffraction simulations further indicate that, despite post-sample space-charge broadening, the essential diffraction features remain intact in the low-charge operating regime considered here.

Overall, these results indicate that compact cryogenic RF photoinjectors can provide a promising path toward next-generation high-brightness MeV-UED systems operating in parameter regimes traditionally associated with significantly larger accelerator facilities. In particular, the combination of high extraction fields and low intrinsic emittance photocathodes enables access to ultrafast, high-coherence electron beams suitable for single-shot diffraction studies of quantum and low-dimensional materials.

ACKNOWLEDGEMENTS

The authors thank M. Kaemingk for pertinent discussions on running the optimizations. This work was supported by the National Science Foundation award No. PHY-1549132.

REFERENCES

[1] W. H. Li *et al.*, "A kiloelectron-volt ultrafast electron microdiffraction apparatus using low emittance semiconductor photocathodes", *Structural Dynamics*, vol. 9, no. 2, p. 024302, 2022. doi:10.1063/4.0000138

[2] D. Filippetto, P. Musumeci, R. K. Li, B. J. Siwick, M. R. Otto, M. Centurion, and J. P. F. Nunes, "Ultrafast electron diffraction: Visualizing dynamic states of matter", *Rev. Mod. Phys.*, vol. 94, no. 4, p. 045004, 2022. doi:10.1103/RevModPhys.94.045004

[3] J. B. Rosenzweig *et al.*, "Next generation high brightness electron beams from ultrahigh field cryogenic rf photocathode sources", *Phys. Rev. Accel. Beams*, vol. 22, no. 2, p. 023403, 2019. doi:10.1103/PhysRevAccelBeams.22.023403

[4] J. B. Rosenzweig *et al.*, "An ultra-compact x-ray free-electron laser," *New J. Phys.*, vol. 22, no. 9, p. 093067, 2020. doi:10.1088/1367-2630/abb16c

[5] R. R. Robles *et al.*, "Versatile, high brightness, cryogenic photoinjector electron source," *Phys. Rev. Accel. Beams*, vol. 24, no. 6, p. 063401, 2021. doi:10.1103/PhysRevAccelBeams.24.063401

[6] A. D. Cahill *et al.*, "High gradient experiments with X-band cryogenic copper accelerating cavities," *Phys. Rev. Accel. Beams*, vol. 21, no. 10, p. 102002, 2018. doi:10.1103/PhysRevAccelBeams.21.102002

[7] A. D. Cahill *et al.*, "Rf losses in a high gradient cryogenic copper cavity," *Phys. Rev. Accel. Beams*, vol. 21, no. 6, p. 061301, 2018. doi:10.1103/PhysRevAccelBeams.21.061301

[8] G. E. Lawler *et al.*, "Improving Cathode Testing with a High-Gradient Cryogenic Normal Conducting RF Photogun," *Instruments*, vol. 8, no. 1, p. 14, 2024. doi:10.3390/instruments8010014

[9] G. E. Lawler *et al.*, "CrYogenic Brightness-Optimized Radiofrequency Gun (CYBORG)," in *Proc. IPAC'22*, Bangkok, Thailand, Jun. 2022, pp. 2544–2547. doi:10.18429/JACoW-IPAC2022-THPOST046

[10] G. E. Lawler *et al.*, "Reduction of dark current at cryogenic temperatures in a high gradient photogun," in *Proc. IPAC'24*, Nashville, TN, USA, May 2024, pp. 523–526. doi:10.18429/JACoW-IPAC2024-MOPR31

[11] D. H. Dowell and J. F. Schmerge, "Quantum efficiency and thermal emittance of metal photocathodes," *Phys. Rev. Spec. Top. Accel. Beams*, vol. 12, p. 074201, 2009. doi:10.1103/PhysRevSTAB.12.074201

[12] S. Karkare *et al.*, "Ultracold Electrons via Near-Threshold Photoemission from Single-Crystal Cu(100)," *Phys. Rev. Lett.*, vol. 125, p. 054801, 2020. doi:10.1103/PhysRevLett.125.054801

[13] E. Prat *et al.*, "Measurements of copper and cesium telluride cathodes in a radio-frequency photoinjector," *Phys. Rev. Spec. Top. Accel. Beams*, vol. 18, no. 4, p. 043401, 2015. doi:10.1103/PhysRevSTAB.18.043401

[14] S. Karkare *et al.*, "Monte Carlo charge transport and photoemission from negative electron affinity GaAs photocathodes," *J. Appl. Phys.*, vol. 113, no. 14, p. 143705, 2013. doi:10.1063/1.4794822

[15] J. Maxson *et al.*, "Measurement of the tradeoff between intrinsic emittance and quantum efficiency from a NaKSb photocathode near threshold," *Appl. Phys. Lett.*, vol. 106, no. 23, p. 234102, 2015. doi:10.1063/1.4922146

[16] L. Cultrera *et al.*, "Cold electron beams from cryocooled, alkali antimonide photocathodes," *Phys. Rev. Spec. Top. Accel. Beams*, vol. 18, no. 11, p. 113401, 2015. doi:10.1103/PhysRevSTAB.18.113401

[17] P. Denham and P. Musumeci, "Space-Charge Aberrations in Single-Shot Time-Resolved Transmission Electron Microscopy," *Phys. Rev. Appl.*, vol. 15, no. 2, p. 024050, 2021. doi:10.1103/PhysRevApplied.15.024050